

Large Eddy Simulation of Realistic Wind Fields in Daytime Atmospheric Boundary Layer

Robert J. Conzemius^a, Evgeni Fedorovich^b

^a*WindLogics, Inc., Grand Rapids, Minnesota, USA, bobc@windlogics.com*

^b*University of Oklahoma, Norman, Oklahoma, USA, fedorovich@ou.edu*

ABSTRACT: We carried out large eddy simulations (LES) of three cases of daytime convective boundary layer (CBL) evolution at two field data collection sites in Oklahoma. Boundary layer depth, mean temperature and wind profiles from LES were compared with sonde, profiler, and lidar observations and with Weather Research and Forecasting (WRF) model predictions. Three methods of accounting for the large scale forcing in the LES were tested: 1) imposing time-constant large-scale pressure gradient force; 2) including temporal changes in the large-scale pressure gradient force and advection of temperature, humidity, and horizontal velocity components; and 3) applying a simpler force-restore technique that assumes the large-scale forcing is directly proportional to the deviation of horizontally averaged LES variables from their observed/modeled counterparts. Comparisons between LES and measurements revealed that the CBL evolution was influenced by large scale heterogeneity in fluxes at the underlying surface that were not included in LES. Additionally, neither temporal changes in the large-scale pressure gradient nor the effects of advection could be neglected. However, the straightforward incorporation of both these forces in the simulations did not greatly improve predictions of the mean flow fields. The force-restore method provided the only reasonably accurate depiction of mean wind, temperature, and humidity profiles.

1 INTRODUCTION

Large eddy simulation (LES) is a powerful numerical technique to study turbulent boundary layer flows, provided that the energy-containing scales of turbulent motion are resolved, and unresolved turbulent motions lie within the inertial subrange. The LES is well-suited for the study of turbulence in idealized boundary layer flows, particularly under unstable (convective) conditions. In practical wind engineering applications, the LES can be a useful tool for examining the effects of turbulence on the mean wind field, which can be reasonably well represented. Provided the external forcings that act on length scales larger than the LES domain are appropriately taken into account, the technique should be able to reproduce the evolution of the mean wind profile relatively accurately because the energy-containing turbulent motions are resolved rather than modeled. To test this approach, we carried out a number of simulations of daytime convective boundary layer (CBL) evolution.

The primary goals of the study are threefold. First, we intend to evaluate LES predictions of the CBL evolution against lidar observations of CBL depth and to additionally compare LES output with radiometer, radar, and radiosonde data to more fully understand the evolution of the mean wind and temperature in the CBL. The second major goal of the present study is to compare the growth of the simulated CBL with that of the observed CBL to understand the relative importance of various factors that determine the CBL growth. Some contributing physical mechanisms, such as entrainment dynamics, might be well simulated, but others, such as large-scale atmospheric vertical motion, might not. Despite its limitations, LES shows promise for simulating real cases, and it will likely have important applications in the future (in particular, to the

wind energy industry) because of its ability to reproduce nonsteady and turbulent atmospheric flows with high temporal and spatial resolution. Thus, identifying successes and drawbacks of LES for actual atmospheric cases is essential for its application.

2 EXPERIMENTAL DESIGN

The study focuses on the analyses of numerical simulation data in comparison with data from atmospheric field experiments that have been performed over the past several years. Atmospheric boundary layer measurements from these field experiments are well-suited for initializing LES and evaluating its output.

2.1 *Field experiment data*

One case for this particular study was a CBL during the 22 MAY 2002 observations taken as a part of the International H₂O Project (IHOP or IHOP_2002) experiment (Weckwerth et al. 2004). The other two cases occurred during two fair weather days of June 2007 at the Southern Great Plains (SGP) Atmospheric Radiation Measurement (ARM) site near Lamont, Oklahoma.

2.1.1 *IHOP Homestead data*

We chose from the IHOP experiment a day in which the wind shear was relatively strong and was a significant contributor to the CBL dynamics (Conzemius and Fedorovich 2006). A vast dataset of observations was available from the IHOP_2002 experiment for this particular case, which presented some of the best conditions during IHOP_2002 for comparing the observed evolution of the sheared atmospheric CBL (Moeng and Sullivan 1994; Pino et al. 2003; Conzemius and Fedorovich 2006) with LES predictions.

During IHOP, intensive profiler, radiosonde, and lidar measurements were taken at a field station about 30 km southwest of Beaver, Oklahoma, which was designated as the Homestead site. Three integrated surface flux facility (ISFF) stations were deployed in the Oklahoma and Texas panhandles along an approximately 50-km long, north-south line centered on the Homestead site. Balloon-borne sounding data were available from nearby National Weather Service (NWS) launch sites at Amarillo, Texas (AMA) and Dodge City, Kansas (DDC). The observational data used for the simulation input also included measurements from the Atmospheric Emitted Radiance Interferometer (AERI) mounted on a 1994 Winnebago (AERIBAGO; Feltz et al. 2003), which was located at the Homestead site. To compare with LES output, CBL depth estimates were available from lidars located at the Homestead site (Guerra et al. 1999; Davis et al. 2000).

2.1.2 *ARM SGP data*

The ARM SGP observational site is located near Lamont, Oklahoma. This site is instrumented with a radiosonde launch facility, radar wind profilers, stations for near-surface turbulent flux measurements through the eddy-correlation technique, and radiometers. For the present study, the Lamont site provided atmospheric sounding data (pressure, temperature, dew point temperature, wind speed and direction) every 6 h, along with 30-min averaged values of near-surface sensible and latent heat fluxes.

2.2 Numerical setup

2.2.1 Initial conditions and general setup features

2.2.1.1 Setup for the IHOP case

The initial wind profile data for the May 22, 2002 case were taken from a combination of the AMA and DDC soundings. Additionally, the large-scale pressure gradient was retrieved from Rapid Update Cycle (RUC; Benjamin et al. 1994) hourly pressure-level analyses, which were retrieved from the National Center for Environmental Prediction (NCEP), in order to calculate geostrophic wind vectors (geostrophic balance occurs when pressure gradient and Coriolis forces are balanced). The profiles of initial wind and geostrophic wind used in the simulation are shown in Fig. 1 together with wind data from the AMA and DDC soundings.

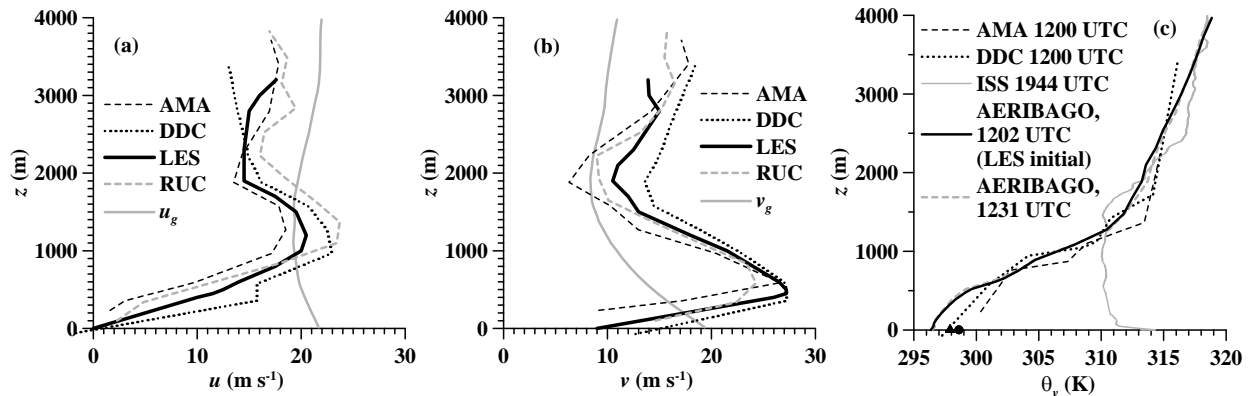


Figure 1. Profiles at 1200 UTC on 22 May 2002: (a) x -component (u), and (b) y -component (v) of the wind (solid gray profile is the initial geostrophic wind taken from the nearest RUC analysis grid point); and (c) virtual potential temperature profiles. The black triangle in (c) indicates the 3-meter virtual potential temperature at the ISFF2 flux site. The black circle is the ISS virtual potential temperature at the Homestead site.

Table 1. Parameters of conducted LES for the May 22, 2002 case

Parameter	Setting
Domain size	$7.68 \times 7.68 \times 3.99 \text{ km}^3$
Grid	$256 \times 256 \times 133$ (30-meter cells)
Starting time	1230 UTC
Time step	Evaluated from a numerical stability constraint
Time advancement	Leapfrog scheme with Asselin filter
Advection and diffusion terms	Centered, second-order finite difference approximations
Lateral boundary conditions	Periodic for all prognostic variables and pressure
Top boundary conditions	Neumann (zero gradient), sponge layer in top 20% of domain
Lower boundary conditions	No-slip; Neumann for temperature, pressure and subgrid TKE; Monin-Obukhov
Subgrid turbulence param.	Subgrid TKE-based after Deardorff (1980)
Grid frame of reference	$u=14 \text{ m s}^{-1}$; $v=10 \text{ m s}^{-1}$

The LES code employed in the present study is described in Conzemius and Fedorovich (2006). The LES settings for the May 22, 2002 case are listed in Table 1. In order to minimize numerical damping of large wavenumber turbulence and to maximize the time step (Conzemius 2004), a moving grid frame of reference was used in the conducted LES runs.

In order to provide a realistic initialization of turbulence, the LES was pre-run for two hours with a weak negative heat flux at the lower surface in order to develop coherent turbulent structures representative of those occurring just after sunrise. The turbulent components of the flow were then saved and added to the initial mean profiles (see Fig. 1) to provide the initial condi-

tions for the main simulation. Further details of the simulations and observations are provided in Conzemius and Fedorovich (2008).

2.2.1.2 Setup for the ARM SGP cases

Two boundary-layer flow cases observed at the Lamont site in June 2007 were chosen based on their meteorological representativeness of late spring / early summer conditions on the U.S. Great Plains. The Dryline Case (DC) of June 7th included strong warming, wind shifts, and moisture changes associated with the passage of a dryline. The Postfrontal Case (PC) of June 8th was preceded by the passage of a cold front in the overnight hours and was characterized by lower temperatures, northerly winds, and stronger static stability across the boundary layer. Simulations for these cases were run in a domain of $51.2 \times 51.2 \times 4 \text{ km}^3$, on a $512 \times 512 \times 80$ grid with uniform horizontal (100 m) and vertical (50 m) spacings.

Complementary to LES, the same boundary layer evolution cases were reproduced by the Weather Research and Forecasting (WRF) model (Skamarock et al. 2008). In the present study we employed the WRF model version 3.0.1 that utilizes the Advanced Research WRF (ARW) dynamical core. The model was run in a domain with horizontal dimensions of $100 \times 100 \text{ km}^2$ and extending to 100hPa in the vertical, or approximately to 16 km. The model equations were solved on a vertically stretched computational grid with horizontal grid spacing of 1 km and three different boundary layer parameterization schemes: YSU (Hong et al. 2006), MYJ (Janjic 2002), and ACM (Pleim 2007). A 12-h warm start was used to allow for model spin-up. Model settings for microphysics, longwave radiation, shortwave radiation, land-surface model, and horizontal diffusion closure were held the same for all runs. The LES and WRF model domains were centered at the wind profiler location within the Lamont ARM site.

2.2.2 Representation of large-scale forcings in LES

Three methods of representing forcings, whose scales were larger than the LES domain, were chosen.

2.2.2.1 Time-constant large scale pressure gradient

Since the LES code employs a formulation for Coriolis force components that expresses these components in terms of the deviation of the flow vector from its geostrophic value, we calculated geostrophic wind vectors for input to the simulation. For the IHOP May 22, 2002 case, the geostrophic wind vectors at 1200, 1500, 1800, and 2100 UTC 22 May and 0000 UTC 23 May were averaged to produce the vertical profile of geostrophic wind vectors that was used throughout the run. The geostrophic wind was taken to be constant in time during the simulation. With the exception of the last 2 h of the simulation, the RUC data showed that pressure gradients changed relatively little during the day on 22 May 2002, so this seems to be a reasonable assumption.

2.2.2.2 Time-varying large scale pressure gradient plus advection

In runs with time-varying large-scale pressure field, the geostrophic wind vectors were calculated and updated hour by hour. The advection forces were calculated explicitly from the RUC grid using a centered, second order finite difference and input as additional advection forces. Advection of potential temperature, humidity, and wind vector components was included, and their values were updated once per hour.

2.2.2.3 Force-restore method

In this case, the Coriolis and large-scale pressure gradients (represented as geostrophic wind vectors) were updated hourly as described in the preceding subsection. However, rather than compute the large-scale advection forcing explicitly, a force-restore method was used in the following formulation:

$$\left(\frac{\partial \tilde{\phi}}{\partial t}\right)_{F-R} = -\frac{\tilde{\phi}(z)_{LES} - \phi(z)_{RUC}}{t_r} \quad \text{with } t_r = 3600\text{s},$$

where t_r is the restore time scale. Thus, for each prognostic filtered variable of LES (except for the vertical velocity component and the subgrid turbulence kinetic energy) $\tilde{\phi}$ evaluated at a given time step, a horizontally averaged vertical profile $\tilde{\phi}(z)_{LES}$ was calculated that was then compared with the corresponding RUC profile $\phi(z)_{RUC}$, and the difference was used as a restoring forcing term (left-hand side of the above equation) at the next time step. The restoring term was applied uniformly with respect to x and y across the entire domain. It is therefore implied that through the force-restore term the large-scale flow imposes control on the mean flow in the LES domain by not allowing mean-flow profiles to deviate too much from their large-scale counterparts, while the CBL flow features on scales smaller than the LES domain size are primarily determined by turbulence mechanisms associated with resolved and subgrid turbulent motions directly reproduced by LES.

3 SIMULATED CBL PARAMETERS COMPARED WITH OBSERVATIONS

The simulated CBL in the IHOP case generally grows more slowly than the observed CBL (Fig. 2). Starting approximately 1830 UTC, the lidar-detected CBL depth increases rather rapidly as a dryline passes over the observation location. A dryline represents the interface between two different CBL types – one relatively shallow, humid, and with lower potential temperature, and the other deeper, drier, and with larger potential temperature. This CBL heterogeneity made it nearly impossible to simulate the May 22, 2002 case with the constraints imposed by using LES periodic boundary conditions. The inclusion of the time-varying large scale pressure gradient force and advection improved the simulated evolution of CBL depth, but the CBL still grew more slowly than it did in the observations.

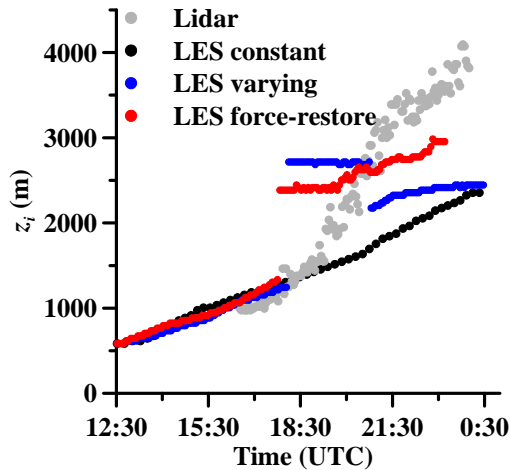


Figure 2. The CBL depth z_i as a function of time for the three simulations. The time-constant pressure gradient simulation is noted with black dots, the time-varying forcing is noted by the blue dots, and the simulation with the force-restore method is indicated with red dots. Lidar-determined CBL depths (Guerra et al. 1999; Davis et al. 2000) are noted with gray dots.

One must additionally note that, in the case under consideration, the sharp gradients in CBL depth, potential temperature, and humidity also cannot be faithfully represented in the RUC analyses, which, in this case, have a 20-km grid spacing. Even with the force-restore method, evolution of the simulated CBL depth does not match the CBL growth evaluated from the vertical profiles of lidar backscatter. In fact, the simulated depth values fall approximately halfway in-between the original simulation data and the lidar-determined CBL depth. Due to the fact that the dryline was located almost exactly over the Homestead site (Demoz et al. 2006; Weiss et al. 2006), the RUC analyses likely smooth the gradient in CBL depth such that the RUC-analyzed CBL characteristics over the Homestead site fall between those of the cooler, shallower, and more humid CBL to the east of the site and the drier, warmer, and deeper CBL to the west. Overall, none of the three methods to account for the large-scale forcing proved capable of fully handling the effects of heterogeneous CBL conditions because LES boundary conditions were periodic.

The conducted simulations showed that the force-restore method worked best to simulate the CBL mean flow structure (Fig. 3), which is probably expectable. Due to the nonlinear nature of the advection terms, calculating them once per hour from RUC analyses is not frequent enough to sufficiently characterize their behavior during the simulation. Without calculating these terms from the full 3-D fields as in the larger-scale models, their effects on the flow cannot be properly represented in the simulations, and it is probably best to revert to the simpler force-restore method to reproduce the mean flow-structure more or less accurately.

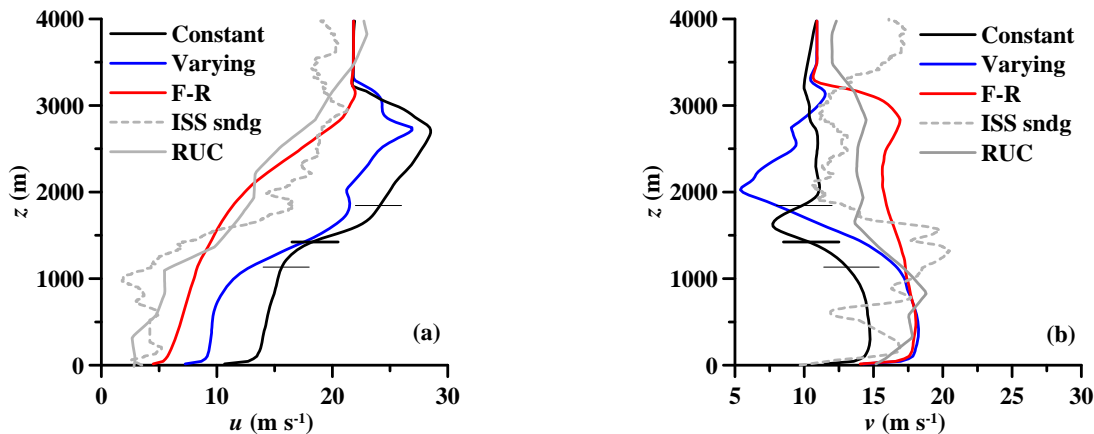


Figure 3. Comparisons between profiles of velocity components (a) u and (b) v predicted by the three simulations with large scale pressure gradients constant in time (solid black), varying large scale pressure gradients and advection forces (blue), and using the force-restore method (red). The corresponding ISS sounding (dashed gray) and RUC 2000 UTC analysis (solid gray) are also shown.

The force-restore type forcing worked the best also for Lamont CBL cases. Obtained mean profiles of temperature, humidity, and wind components were in general agreement with the sounding data and wind profiler data (not shown) from the Lamont site during the daytime stages of the boundary layer development. Simulated CBL evolution patterns for the DC and PC cases are presented in Fig. 4 along with predictions by the WRF model using three different boundary-layer parameterization schemes. In the first CBL case (June 7), characterized by a comparatively strong nonstationarity of the CBL driving mechanisms, WRF model predicts much stronger variations in the CBL depth than the LES. As for the discrepancies between LES estimates of the CBL depth using different methods, those may be explained by the disconnection between the heat (virtual temperature) flux and vertical organization of the mean potential temperature field

during morning and evening hours when the levels of maximum vertical temperature gradient and minimum heat flux in the CBL are not collocated.

It remains unclear how to meaningfully introduce the larger-scale forcing terms into the filtered LES prognostic equations. Technically, these terms are already larger than the filter scale, so there is an additional separation between the resolved turbulent motions on the grid and the larger-than-domain-scale motions. Although the force-restore method might seem rather crude, it seems to account for all of these unknown terms in a sufficient manner.

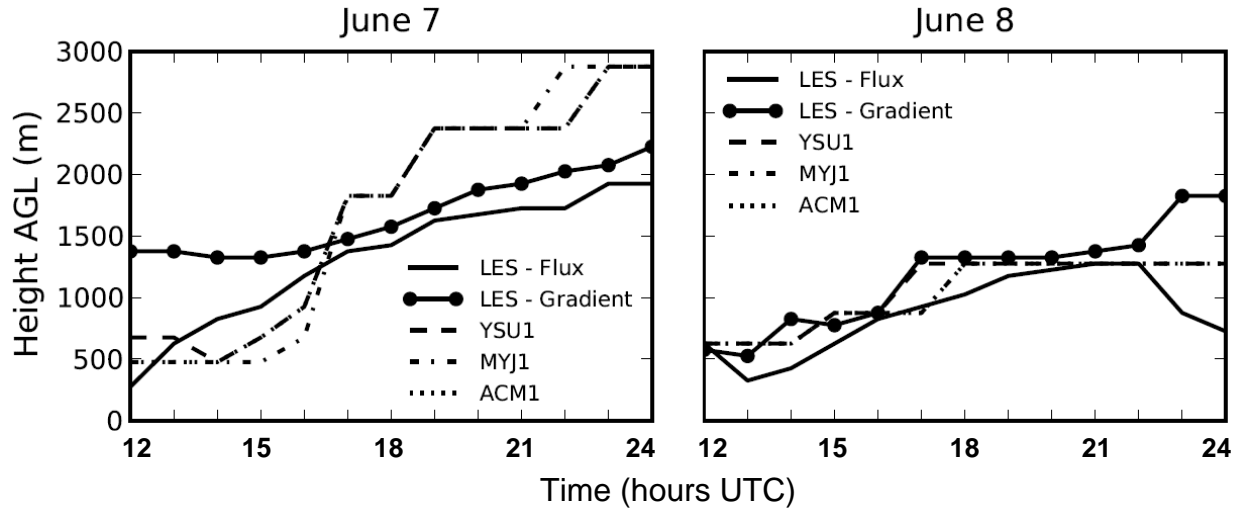


Figure 4. Boundary layer depth evolution at the Lamont site in the DC case (left) and PC case (right). The LES data are obtained with nudging (force-restore method) and the CBL top height is estimated from the elevation of the maximum temperature gradient (LES – Gradient) and minimum of the heat flux (LES – Flux). Three other lines represent WRF model data obtained with three different boundary-layer schemes (YSU, MYJ, and ACM).

4 SUMMARY AND CONCLUSIONS

In the May 22, 2002 case, the CBL evolves more slowly with time in the original simulations than in the observations. This discrepancy can be explained by the approach of a dryline – the interface between two CBLs of greatly different temperature, and moisture content. Such interfaces are hard to simulate due to the constraints imposed by lateral boundary conditions in LES, which are usually chosen as periodic. Simulations with advection and the time variation of large scale pressure gradients included in the LES equations did not show an appreciable improvement in the ability of the simulation to reproduce the evolution of the observed CBL. This may be mostly due to the insufficiently frequent update of the advection terms calculated from hourly analyses. The prescription of the larger scale terms within the LES equations of motion is also difficult to formalize. The meanings of the additional terms that result are unclear. Rather, the best method to reproduce the observed CBL evolution is apparently through a force-restore term, applied to the LES horizontally averaged profiles. This allows the adjustment of the mean flow profiles in the LES domain to the large-scale flow fields on a time scale that is larger than the convective time scale of the CBL, with local flow features within the domain being controlled by internal LES mechanisms.

5 ACKNOWLEDGEMENTS

The research presented here was supported by National Science Foundation grant ATM-0124068 and by a grant from the Netherlands Organization for Applied Research (TNO).

6 REFERENCES

Journal papers:

- Conzemius, R. J., Fedorovich, E., 2006. Dynamics of sheared convective boundary layer entrainment. Part I: methodological background and large eddy simulations, *Journal of the Atmospheric Sciences* 63, 1151-1178.
- Conzemius, R. J., Fedorovich, E., 2008. A case study of convective boundary layer development during IHOP: numerical simulations compared to observations, *Monthly Weather Review* 136, 2305-2320.
- Deardorff, J. W., 1980. Stratocumulus-capped mixed layers derived from a three-dimensional model, *Boundary-Layer Meteorology* 18, 495-527.
- Davis, K. J., Gamage, N., Hagelberg, C. R., Kiemle, C., Lenschow, H., Sullivan, P. P., 2000. An objective method for deriving atmospheric structure from airborne lidar observations. *Journal of the Atmospheric Sciences* 17, 1455-1468.
- Demoz, B., and Coauthors, 2006. The dryline on 22 May 2002 during IHOP_2002: convective-scale measurements at the profiling site, *Monthly Weather Review* 134, 294-310.
- Feltz, W. F., Howell, H. B., Knuteson, R. O., Woolf, H. M., Revercomb, H. E., 2003. Near continuous profiling of temperature, moisture, and atmospheric stability using the atmospheric emitted radiance interferometer (AERI), *Journal of Applied Meteorology* 42, 584-597.
- Guerra, D., Schwemmer, G., Wooten, A., Chaudhuri, S., Wilkerson, T., 1999. Prototype holographic atmospheric scanner for environmental remote sensing, *Journal of Geophysical Research* 104 (D), 22287-22292.
- Hong, S., Noh, Y., Dudhia, J., 2006. A new vertical diffusion package with an explicit treatment of entrainment processes. *Monthly Weather Review* 134, 2318-2341.
- Moeng, C.-H., Sullivan, P. P., 1994. A comparison of shear- and buoyancy-driven planetary boundary layer flows. *Journal of the Atmospheric Sciences* 51, 999-1022.
- Pino, D., de Arellano, J. V.-G., Duynkerke, P. J., 2003. The contribution of shear to the evolution of a convective boundary layer. *Journal of the Atmospheric Sciences* 60, 1913-1926.
- Pleim, J. E., 2007. A combined local and non-local closure model for the atmospheric boundary layer. Part 1: Model description and testing, *Journal of Applied Meteorology and Climatology* 46, 1383-1395.
- Weckwerth, and Coauthors, 2004. An overview of the International H₂O Project (IHOP_2002) and some preliminary highlights, *Bulletin of the American Meteorological Society* 85, 253-277.
- Weiss, C., Bluestein, H. B., Pazmany, A. L., 2006. Finescale radar observations of the 22 May 2002 dryline during the International H₂O Project (IHOP), *Monthly Weather Review* 134, 273-293.

Monographs, Multi-author volumes, Proceedings:

- Benjamin, S. G., Brundage K. J., Morone L. L., 1994: Implementation of the Rapid Update Cycle. Part I: Analysis/Model Description, Tech. rep., NOAA, USA.
- Conzemius, R. J., 2004. The effects of wind shear on the convective boundary layer entrainment, Ph.D. dissertation, University of Oklahoma, 338 pp.
- Janjic, Z. I., 2002: Nonsingular Implementation of the Mellor-Yamada 2.5 Scheme in the NCEP Meso Model. Tech. rep., NCEP, USA.
- Skamarock W. C., Klemp, J. B., Dudhia, J., Gill, D. O., Barker, D. M., Wang, W., Powers, J. G., 2008. A Description of the Advanced ResearchWRF Version 3, Tech. rep., NCAR, USA.